Biomedical Signal Processing and Control 105 (2025) 107649

Contents lists available at ScienceDirect

Biomedical Signal Processing and Control

journal homepage: www.elsevier.com/locate/bspc

Control of end-tidal carbon dioxide during phrenic nerve stimulation with mechanical ventilation

Arnhold Lohse [a,*], Felix Röhren [a], Philip von Platen [a], Carl-Friedrich Benner [a], Dmitrij Ziles [b], Marius Hühn [b], Matthias Manfred Deininger [b], Thomas Breuer [b], Steffen Leonhardt [a], Marian Walter [a]

[a] Chair for Medical Information Technology, RWTH Aachen University, Pauwelsstraße 20, 52074, Aachen, Germany
[b] Department of Intensive and Intermediate Care, Medical Faculty, RWTH Aachen University, Pauwelsstraße 30, 52074, Aachen, Germany

ARTICLE INFO

Keywords:
Phrenic nerve stimulation
Mechanical ventilation
Robust control
Functional electric stimulation
Physiological closed-loop control

ABSTRACT

Mechanical ventilation maintains the gas exchange of patients in the intensive care unit which is life-saving, but prolonged ventilation results in diaphragm atrophy. Phrenic nerve stimulation can keep the diaphragm active so that atrophy might be avoided. To use phrenic nerve stimulation in a clinical setting, it is important to implement a closed-loop control system that automatically adjusts stimulation parameters to achieve the desired ventilation. This study presents the development of a robust cascaded control system for end-tidal carbon dioxide using phrenic nerve stimulation. The control system was validated in simulations with 100 virtual patients, in which the conditions of the phrenic nerve stimulation and the patient's condition changed, as well as in animal trials using pigs. The control system proved to be robust to end-tidal carbon dioxide perturbations, such as changing stimulation efficiency, varying patient conditions, and disconnection, in both simulations and animal trials. Regarding reference tracking, the control system achieved a settling time of 5.5 min–14 min in simulations and of 7.3 min–38.8 min in animal trials. The proposed control system can be used for further development of feedback-controlled phrenic nerve stimulation in the intensive care unit.

1. Introduction

Mechanical ventilation is used to treat patients with respiratory insufficiencies in the intensive care unit (ICU). Following the successful treatment of the underlying respiratory failure, patients typically undergo weaning [1], where they exercise spontaneous breathing, particularly to strengthen the respiratory muscles to recover from the mechanical ventilator. However, one risk of mechanical ventilation is ventilator-induced diaphragmatic dysfunction (VIDD) [2], in which patients develop diaphragm atrophy, directly impacting the weaning outcome [3]. When a patient's respiratory force is insufficient for adequate breathing, it results in weaning failure, leading to prolonged hospital stays and reduced survival rates [4]. A promising approach to mitigating VIDD is PNS, as it triggers artificial diaphragmatic contractions to prevent diaphragmatic atrophy. Furthermore, a combination of PNS and mechanical ventilation was also suggested [5].

For future clinical applications in the ICU, a control system that automatically adjusts PNS settings to achieve the ventilation target is essential. So far, few studies have been conducted on PNS or respiratory pacing with feedback. It has been demonstrated that PNS or diaphragm stimulation can be triggered by measuring the airway flow or the diaphragm electromyography [6–8]. Regarding PNS, an optimization of stimulation amplitude and frequency was proposed by Zhou et al. [9]. Similarly, Keogh et al. [10] developed a closed-loop PNS system that automatically identifies the most effective stimulation settings and surface electrode configuration based on the respiratory response of healthy volunteers.

Various control strategies for mechanical ventilation have been developed [11] that, e.g., control the end-tidal partial CO_2 pressure (P_{etCO_2}) [12]. In contrast, there are only a few PNS studies with objectives similar to those in mechanical ventilation. Ai et al. [13] introduced a closed-loop respiratory pacemaker framework that controls arterial O_2 saturation of hemoglobin through a proportional-integrative (PI) controller validated using a computational model. Inspired by biology, Siu et al. [14] developed a neural-network based closed-loop diaphragm pacing system that tracks volume profiles and was validated in rats. Additionally, the system was utilized with concurrent stimulation of the diaphragm and intercostal muscles at the same time [15].

* Corresponding author.
E-mail address: lohse@hia.rwth-aachen.de (A. Lohse).

https://doi.org/10.1016/j.bspc.2025.107649
Received 24 September 2024; Received in revised form 14 January 2025; Accepted 31 January 2025
Available online 12 February 2025

Table 1
Summary of recent studies on respiratory pacing with feedback. Models denote a computational model used in simulations; duration refers to the length of respiratory pacing.

Objective	Stimulation type.	Subject	Duration	Ref.
Arterial O_2 saturation control	Unspecified, PNS	Model	–	[13]
Bio-inspired volume control	Implanted diaphragmatic stim.	Rats	100–200 breaths	[14]
Bio-inspired volume control	Implanted diaphragmatic and intercostal muscle stim.	Rats	5–15 min	[15]
Bio-inspired P_{etCO_2} and flow control	Implanted diaphragmatic stim.	Model	–	[16]
Bio-inspired P_{etCO_2} and flow control	Implanted diaphragmatic stim.	Rats	≥15 min	[17]

Similarly, Zbrzenski et al. [16] and Siu et al. [17] developed a bio-inspired neural-network based control system that acts on P_{etCO_2} and flow. A summary of these studies can be found in Table 1.

In order to ensure the safe use of controlled PNS in the ICU, additional measures are required to comply with the relevant medical regulations. Before clinical application, PNS control systems need to be validated in humans, but as a preliminary step, pigs can be used as their cardiorespiratory system is comparable to those of humans [18]. Moreover, Reardon et al. [19] suggested that PNS may prove to be an optimal strategy for artificial breathing if diaphragm activity is maintained within lung-protective range, which has been formulated to prevent lung injury [20]. During prolonged application of PNS and mechanical ventilation, the control system must react adequately to dynamic changes in the patient's condition, e.g. due to variations in secretion or vigilance. Furthermore, depending on the electrode placement method, position changes of the electrodes might influence PNS over time. This is exemplified by our proposed minimal-invasive percutaneous electrode placement near the phrenic nerve [21].

This paper presents a novel PNS control system for end-tidal partial CO_2 pressure P_{etCO_2}, developed with the specific needs of intensive care personnel in mind. It has been designed to ensure transparent and comprehensible behavior in compliance with relevant medical regulations. In order to fulfill the criteria for lung-protective ventilation outlined in recent literature [20,22], a cascaded controller structure was selected. The controllers were designed to be robust against dynamic changes by employing $\mathcal{H}_\infty$ synthesis. Given the potential safety concerns associated with system complexity and lack of transparency in automated therapies [23], the synthesized controllers were designed with a simple PI structure in which the effect of each parameter is interpretable. Additionally, the control system provides pressure support as a fail-safe measure in the case that PNS alone does not provide adequate ventilation. The control system was systematically validated through simulations of varying patient conditions with a model different from the one employed in $\mathcal{H}_\infty$ synthesis to verify robustness. Subsequently, the system was validated in four pigs that received percutaneous PNS for 96 h under the supervision of human intensive care physicians. Additionally, the system was validated in a fifth pig in which PNS was applied after an initial mechanical ventilation period of 72 h.

2. Methods

2.1. Process overview of phrenic nerve stimulation

The experimental setup of PNS is illustrated in Fig. 1 [24]. A host computer communicates with an embedded computer (*dSPACE Microlabbox*, dSPACE GmbH, Paderborn, Germany) that has been programmed with *Matlab Simulink 2019b* (The MathWorks Inc., Natick, USA). The embedded computer is linked to a modified mechanical ventilator (EVE IN, Fritz Stephan GmbH, Gackenbach, Germany) via an RS-232 protocol that applies pressure to the patient or pig via a respiration tube. The mechanical ventilator transmits measurement data of airway pressure, airway flow $\dot{V}$, and end-tidal partial CO_2 pressure P_{etCO_2} to the embedded computer. The embedded computer has a digital interface to a custom-built stimulator connected to two electrode pairs placed near the left and right phrenic nerves, as detailed in [21]. The stimulator applied the stimulation voltage υ to the left and right phrenic nerves of the patient, thereby inducing a diaphragm contraction and, therefore, inspiration. In more detail, the stimulation voltage υ forms either alternating or biphasic pulses with the pulse width T_{pw} and the pulse frequency f_p, as given in Fig. 2a.

The pulses form a stimulation burst depicted in Fig. 2b. The pulse voltage amplitude υ_p increases during the slope time T_s from the start amplitude υ_s to the end amplitude υ_e to induce a smoother time contraction. Each pulse burst has a duration of T_b, and the bursts are repeated at the respiratory rate f_{rr}, as each burst indicates stimulated inspiration. Subsequently, no voltage is applied, and the expiration starts. For simplicity in control, υ_s was defined as

$$\upsilon_s = \max\left(\frac{\upsilon_e}{3}, 5\,\mathrm{V}\right). \tag{1}$$

2.2. Control structure

An overview of the control design is given in Fig. 3. Three cascaded control loops were designed. In the outer CO_2 control loop, the reference end-tidal partial CO_2 pressure r_{CO_2} is tracked by adjusting the reference minute volume r_{mv}. In the MV control loop, the respiratory rate f_{rr} and the reference tidal volume r_V are set. In the inner tidal volume V_t control loop, the stimulation voltage parameters υ_e and, if necessary, the pressure support Δp_{ps} are adjusted. Based on its inputs, the stimulator applies the stimulation voltage υ, and the mechanical ventilator applies the airway pressure p_{aw} to the patient. The patient's end-tidal partial pressure of CO_2 y_{CO_2} and the tidal volume y_V are fed back to the controllers. All controllers are robust $\mathcal{H}_\infty$ controllers synthesized with uncertainty models. Each controller was equipped with a clamping anti-windup method [25]. To design a patient-independent controller, the tidal volume and minute volume are scaled by the body weight m so that their unit is mL/kg. If the measured tidal volume is above 20 mL/kg, a disconnection is assumed, and the controllers maintain their previous values.

2.3. End-tidal carbon dioxide control

The control loop for the synthesis of the CO_2 controller is given in Fig. 4. The controller K_{CO_2} sets a reference minute volume r_{MV}, which is achieved by the internal control loops. The inner control loops must have a higher bandwidth than the outer control loop [26] due to the cascaded control structure. The model plant consists of a dead space efficiency gain $\widetilde{k}_D$ and a linearized gas exchange model $G_{CO_2}(s)$.

Based on the relation between total ventilation, dead space ventilation, and alveolar ventilation [27, p. 19], the ventilation efficiency $\widetilde{k}_D$ was modeled as

$$\widetilde{k}_D = \frac{V_t - V_D}{V_t}. \tag{2}$$

A tidal volume V_t in between 6 mL/kg and 8 mL/kg (inside lung-protective range) and a dead space volume V_D between 1.5 mL/kg and 2.5 mL/kg were assumed. The output of $\widetilde{k}_D$ is the alveolar minute

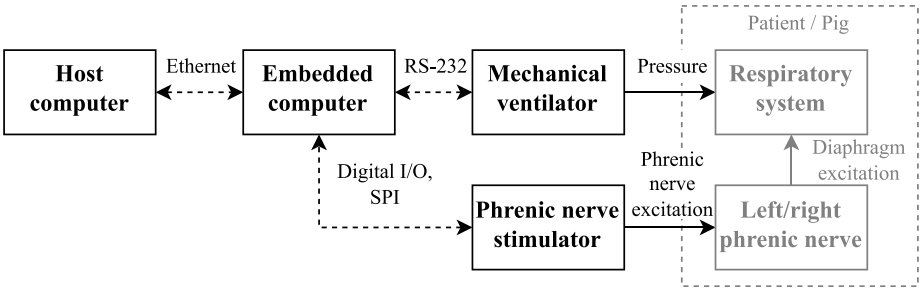

Fig. 1. Experimental setup of PNS.

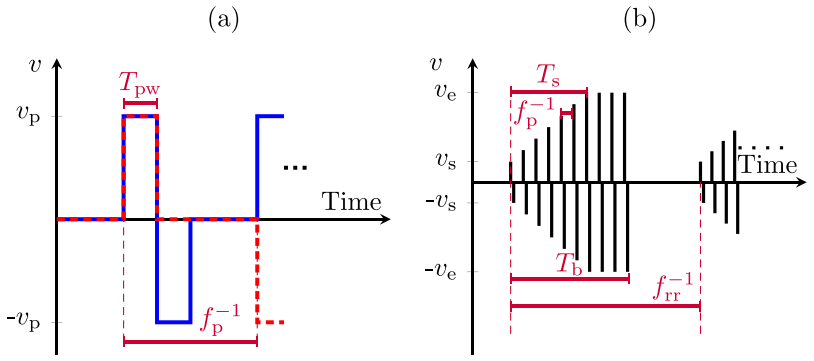

Fig. 2. PNS parameters of a pulse (a). The blue line denotes a biphasic pulse, while the red line denotes an alternating burst. (b) PNS parameters of a burst. *Source:* Adapted from [24].

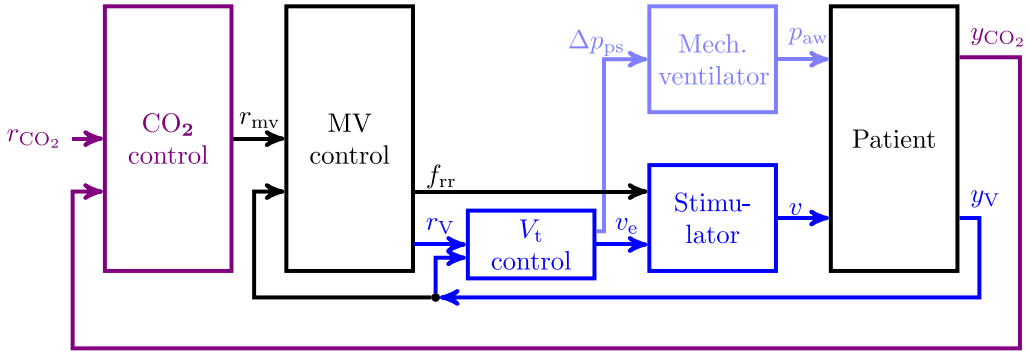

Fig. 3. Overview of the control system with the carbon dioxide CO_2 loop (purple), the minute volume MV loop (black), and the tidal volume V_t loop (blue).

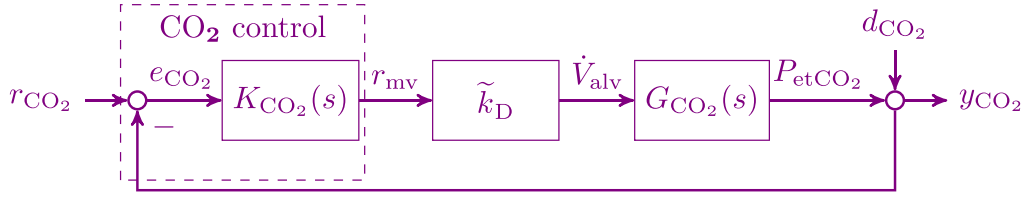

Fig. 4. CO_2 control loop for synthesis.

volume $\dot{V}_{alv}$, which is the input of the nonlinear gas exchange model from Fincham and Tehrani [28]. The model was simplified by reducing it to the alveolar compartment for oxygen and carbon dioxide, the tissue and brain tissue compartment, and the blood transport delay. The details are provided in the supplementary material Section 1.1.

For uncertainty modeling, the model parameters were pseudo-randomized 100 times using the Latin hypercube method [29, p. 76], according to the supplementary material Tab. 1. For each parameter set, the model was trimmed to the nearest equilibrium point, leading to the sampled plants $G_{CO_2,i}(s), i \in \{1, \dots, 100\}$.

With the established uncertainty model, a continuous PI controller was synthesized via the $\mathcal{H}_\infty$ mixed-sensitivity approach, as proposed by Skogestad and Postlethwaite [30, p. 109]. This approach depends on the sensitivity transfer function $S_{CO_2,i}(s)$

$$S_{CO_2,i}(s) = \left(G_{CO_2,i}(s) K_{CO_2}(s)\right)^{-1}, \tag{3}$$

which corresponds to the transfer function from the disturbance input d_{CO_2} to the output y_{CO_2} of the ith sample plant. The complementary

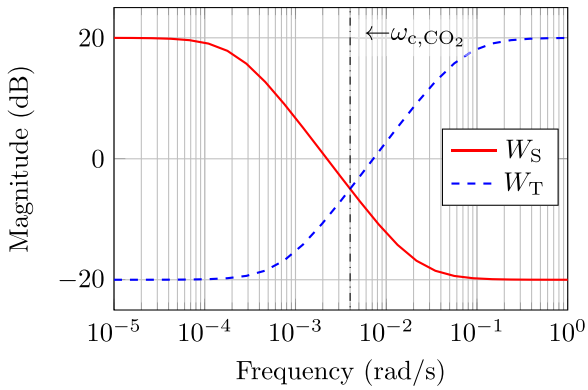

Fig. 5. Weighting functions $W_S(s)$ and $W_T(s)$ of the mixed-sensitivity $\mathcal{H}_\infty$ synthesis for the CO_2 loop.

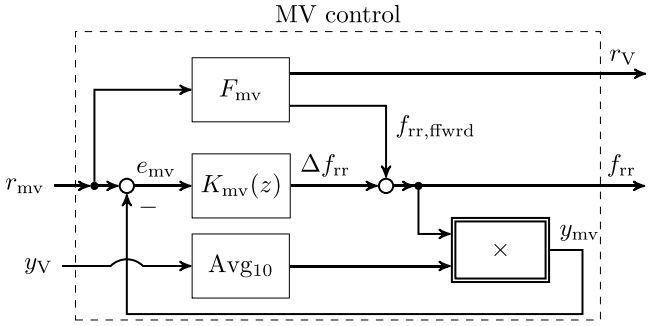

Fig. 6. Minute volume control structure. Avg_{10} denotes the moving average filter of y_V with a length of 10 breaths.

transfer function $T_{CO_2,i}(s)$

$$T_{CO_2,i}(s) = G_{CO_2,i}(s)K_{CO_2}(s)\left(G_{CO_2,i}(s)K_{CO_2}(s)\right)^{-1} \tag{4}$$

is the transfer function from the reference input r_{CO_2} to y_{CO_2} for the ith sample plant. The $\mathcal{H}_\infty$ mixed-sensitivity approach minimizes the cost function

$$\left\| \begin{matrix} W_S(s)S_{CO_2,1}(s) \\ \vdots \\ W_S(s)S_{CO_2,100}(s) \\ W_T(s)T_{CO_2,1}(s) \\ \vdots \\ W_T(s)T_{CO_2,100}(s) \end{matrix} \right\|_\infty , \tag{5}$$

where W_S and W_T denote the weighting functions for the sensitivity and complementary sensitivity functions, respectively. The chosen weighting functions are shown in Fig. 5. W_S is high in frequency regions where disturbance rejection is the prior goal, whereas W_T is high where reference should not be tracked to limit controller aggression. The target cross frequency was selected as $\omega_{c,CO_2} = 4.0 \times 10^{-3}$ rad/s, so that $\left(\omega_{c,CO_2}/(2\pi) \cdot 60\,\text{s/min}\right)^{-1} \approx 26$ min. Based on ω_{c,CO_2}, W_S crossed the 0 dB line at $\omega_{c,CO_2}/1.8$ and W_T at $1.8\,\omega_{c,CO_2}$, respectively. The controllers were synthesized by the command `hinfstruct` in *MATLAB 2021b*.

2.4. Minute volume control

The MV control structure is shown in Fig. 6. Since lower tidal volumes have been associated with better clinical results [22], the control system should first increase the respiratory rate and then the tidal volume. The reference tidal volume r_V is set via feed-forward control F_{mv}, which is dependent on the reference minute volume r_{mv}

$$r_V = \begin{cases} \overline{V}_t & , \ \overline{V}_t \le \frac{r_{mv}}{\overline{f}_{rr}} \\ \frac{r_{mv}}{\overline{f}_{rr}} & , \ \underline{V}_t \le \frac{r_{mv}}{\overline{f}_{rr}} < \overline{V}_t \\ \underline{V}_t & , \ \text{otherwise.} \end{cases} \tag{6}$$

$\overline{f}_{rr}$ denotes the maximum respiratory rate that can be adjusted by the user. Retaining the lung protective guidelines, the lower limit $\underline{V}_t$ and upper limit $\overline{V}_t$ were set to 6 mL/kg and 8 mL/kg, respectively. Depending on r_V, the feed-forward respiratory rate $f_{rr,ffwrd}$ is set as

$$f_{rr,ffwrd} = \begin{cases} \frac{r_{mv}}{\underline{V}_t} & , \ r_V = \underline{V}_t \\ \overline{f}_{rr} & , \ \text{otherwise.} \end{cases} \tag{7}$$

If pressure support is enabled, as explained later in Section 2.5, the lower tidal volume limit $\underline{V}_t$ was set to 4 mL/kg so that the control system decreased pressure support rather than f_{rr}.

If the desired tidal volume cannot be reached, r_{mv} can be achieved by changing the respiratory rate f_{rr} by Δf_{rr}. Because the controller $K_{mv}(z)$ reacts after each recorded tidal volume, $K_{mv}(z)$ is discrete with no constant sample time but reacts after each breath. The measured minute volume y_{mv} is the product of f_{rr} and y_V, where y_V is processed using a moving average filter of 10 breaths. Analogous to the CO_2 control loop, $K_{mv}(z)$ is a PI controller designed by mixed-sensitivity $\mathcal{H}_\infty$ synthesis with the open-loop transfer function $\widetilde{L}_{mv}(z)$

$$\widetilde{L}_{mv}(z) = K_{mv}(z)\,\widetilde{k}_{mv}, \tag{8}$$

where $\widetilde{k}_{mv}$ is the tidal volume between 4 mL/kg and 7 mL/kg. The value range was chosen around $r_V = 6$ mL/kg, where the controller is active. The weighting functions W_S and W_T were defined as in Section 2.3, but with a cross frequency of 3.2×10^{-2} rad/breath. Assuming a f_{rr} in between 20 min^{-1} and 30 min^{-1}, the chosen bandwidth is about 3 to 4 times faster than ω_{c,CO_2} of the end-tidal CO_2 controller. It should be noted that the feed-forward term F_{mv} is dominant compared with $K_{mv}(z)$.

2.5. Tidal volume control

The tidal volume control of stimulation was designed with GPR models $V_{t,gpr}(v_e)$ based on our previous work [31]. The GPR models estimate the relationship between the tidal volume and the maximum stimulation amplitude v_e for one complete breath. An illustrative example of such a GPR model is depicted in Fig. 7. From the resulting 33 GPR models, the gradient $k_V = \frac{dV_t}{dv_e}$ was determined. For each stimulation voltage setting j, the respective gradient k_V was calculated by

$$k_V(j) = \frac{1}{2}\left(\frac{V_t(j+1) - V_t(j)}{v_e(j+1) - v_e(j)} + \frac{V_t(j) - V_t(j-1)}{v_e(j) - v_e(j-1)}\right). \tag{9}$$

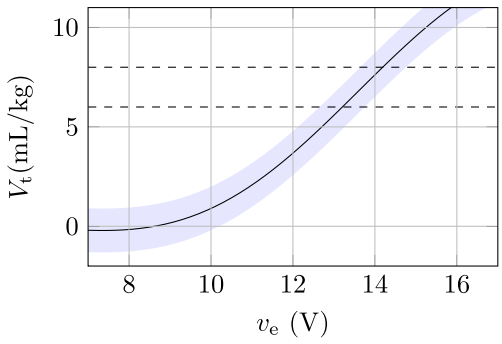

Fig. 7. Illustrative GPR model. The blue area denotes the 95% confidence interval. The dashed lines denote the reference limits of 6 mL/kg and 8 mL/kg. For v_e below 7 V, V_t was zero.

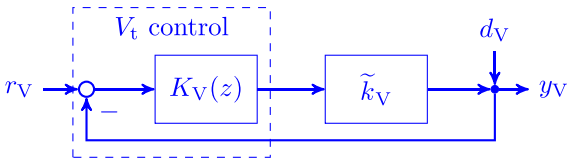

Fig. 8. Tidal volume control loop for synthesis.

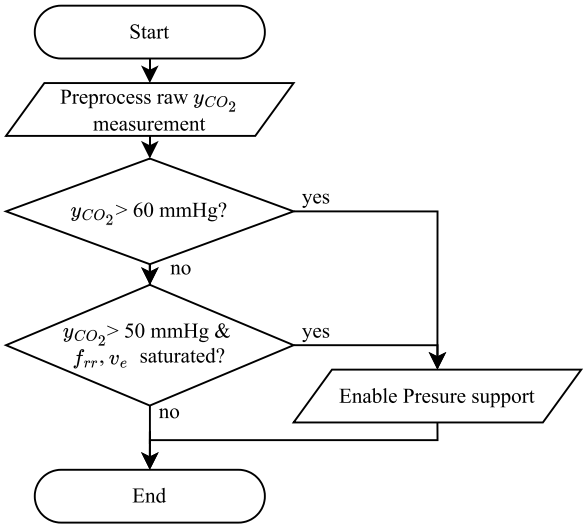

Fig. 9. Program flowchart on how pressure support is enabled. During preprocessing, invalid y_{CO_2} measurement values are sorted out, and a moving average filter with a length of ten breaths is applied. Pressure support can only be manually disabled.

As a result, the nominal gain of k_V was found to be the median of 0.6 mL kg^{-1} V^{-1}, and the maximum value was the maximum observed gain of 5.0 mL kg^{-1} V^{-1}. The minimum value was defined as 0.2 mL kg^{-1} V^{-1} to avoid gains near zero, which can cause problems during control synthesis. These ranges were used to define the uncertain gain $\widetilde{k}_V$ and synthesize $K_V(z)$ via mixed-sensitivity $\mathcal{H}_\infty$ synthesis. Similar to $K_{mv}(z)$, $K_V(z)$ is discrete and reacts after each breath. The desired bandwidth was 0.11 rad/breath, so that process noise during PNS, modeled as a disturbance impulse d_V of 1 mL/kg, change v_e less than 0.05 V. Further, this bandwidth is approximately 9 to 14 times faster than ω_{c,CO_2} for f_{rr} in between 20 min^{-1} and 30 min^{-1}. The block diagram of this control loop is provided in Fig. 8. The v_e maximum of 20 V can be decreased by the user if a further increase of v_e does not result in a higher V_t.

As shown in Fig. 3, if PNS-based respiration is insufficient, pressure support is enabled. The conditions for enabling pressure support are shown in Fig. 9. In addition, manual activation of pressure support is possible.

Similar to the PI controller that adjusts v_e, the pressure support controller was synthesized via the $\mathcal{H}_\infty$ mixed-sensitivity approach with an uncertain gain $\widetilde{k}_{ps}$ given by

$$\widetilde{k}_{ps} = \frac{\widetilde{C}}{\widetilde{m}} \quad . \tag{10}$$

Using data from preliminary animal trials, the uncertain respiratory compliance $\widetilde{C}$ was estimated to be between 15 mL hPa^{-1} kg^{-1} and 30 mL hPa^{-1} kg^{-1}, while the pig's body weight $\widetilde{m}$ lied between 40 kg and 50 kg, as defined in the test protocol. The cross frequency was chosen as 0.07 rad/breath so that it is 9 times faster than ω_{c,CO_2} at $f_{rr} = 30$ min^{-1}.

In addition to maintaining the exchange of CO_2, minimizing the required pressure support is a defined goal. Therefore, if pressure support must be enabled, f_{rr} and v_e remain at their maximum and

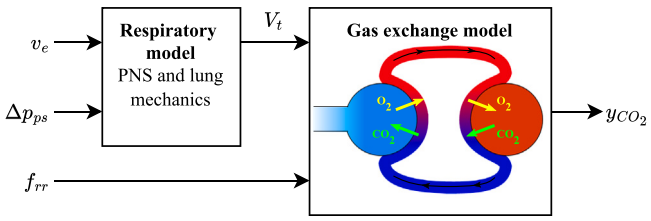

Fig. 10. Respiratory and gas exchange model for simulation.

can only decrease if the pressure support Δp_{ps} is zero. All synthesized control parameter values are given in supplementary material Tab. 2.

2.6. Simulation

2.6.1. Validation model

For validation, a different model shown in Fig. 10 was used to avoid designing controllers tailored to a specific model. The respiratory model combines PNS and pressure support, so that V_t is given by

$$V_t = V_{t,pns}(v_e) + C\Delta p_{ps} + w, \tag{11}$$

where $V_{t,pns}(v_e)$ denotes the tidal volume generated by PNS dependent on v_e. The underlying physiological model [32] is described in supplementary material Section 2.1. A white process noise w was added to capture the variation in tidal volume of individual breaths. The standard deviation was set at 0.51 mL/kg such that ±1.0 mL/kg defines the 95% confidence interval. V_t was used along with f_{rr} as an input of the gas exchange model. The gas exchange model described in supplementary material Section 2.2, based on Batzel et al. [33] and Spencer [34] was modified from our publication [35]. The gas exchange model output y_{CO_2} is P_{etCO_2}.

2.6.2. Robustness validation

In physiological models, many parameters are patient-specific. To validate the robustness of the control system, all patient- and time-varying parameters were varied. While most of the value ranges are given by values taken from literature [28,33,34,36–38], supplementary material Section 2.3 explains how each parameter range was defined. Given the parameter ranges, 100 virtual patients were generated via Latin-Hypercube sampling and simulated in the scenario defined in Table A.1. The scenario contains an r_{CO_2} reference step, a disconnection, and dynamic fluctuations in V_D, $\dot{V}_{mr,CO_2}$, and Q_{co}. The metabolic CO_2 production rate $\dot{V}_{mr,CO_2}$ values were obtained from [39,40], and the cardiac output Q_{co} values were taken from [41]. Moreover, the input and output PNS efficiency were modified. A reduction in the input PNS efficiency by 80% means that in Eq. (11), $V_{t,gpr}(v_e)$ is substituted by $V_{t,gpr}(0.2v_e)$, while a reduction in PNS output efficiency is $0.2V_{t,gpr}(v_e)$.

2.7. Experimental validation

The developed control system was validated in animal trials with five healthy pigs (German Landrace, female, between 40 kg and 50 kg) that were stimulated or mechanically ventilated for 96 h. The mechanical ventilator operated in continuous positive airway pressure mode with optional pressure support during PNS. The inputs and settings of the control system and the applied continuous airway pressure were adjusted according to the pig's needs. PNS patterns were selected from our published systematic evaluation [24] and are listed in Table 2. PNS patterns with lower pulse widths T_{pw} and pulse frequencies f_p were preferred, but if the tidal volume achieved without pressure support was inadequate, the next PNS pattern that achieved higher tidal volumes was manually selected.

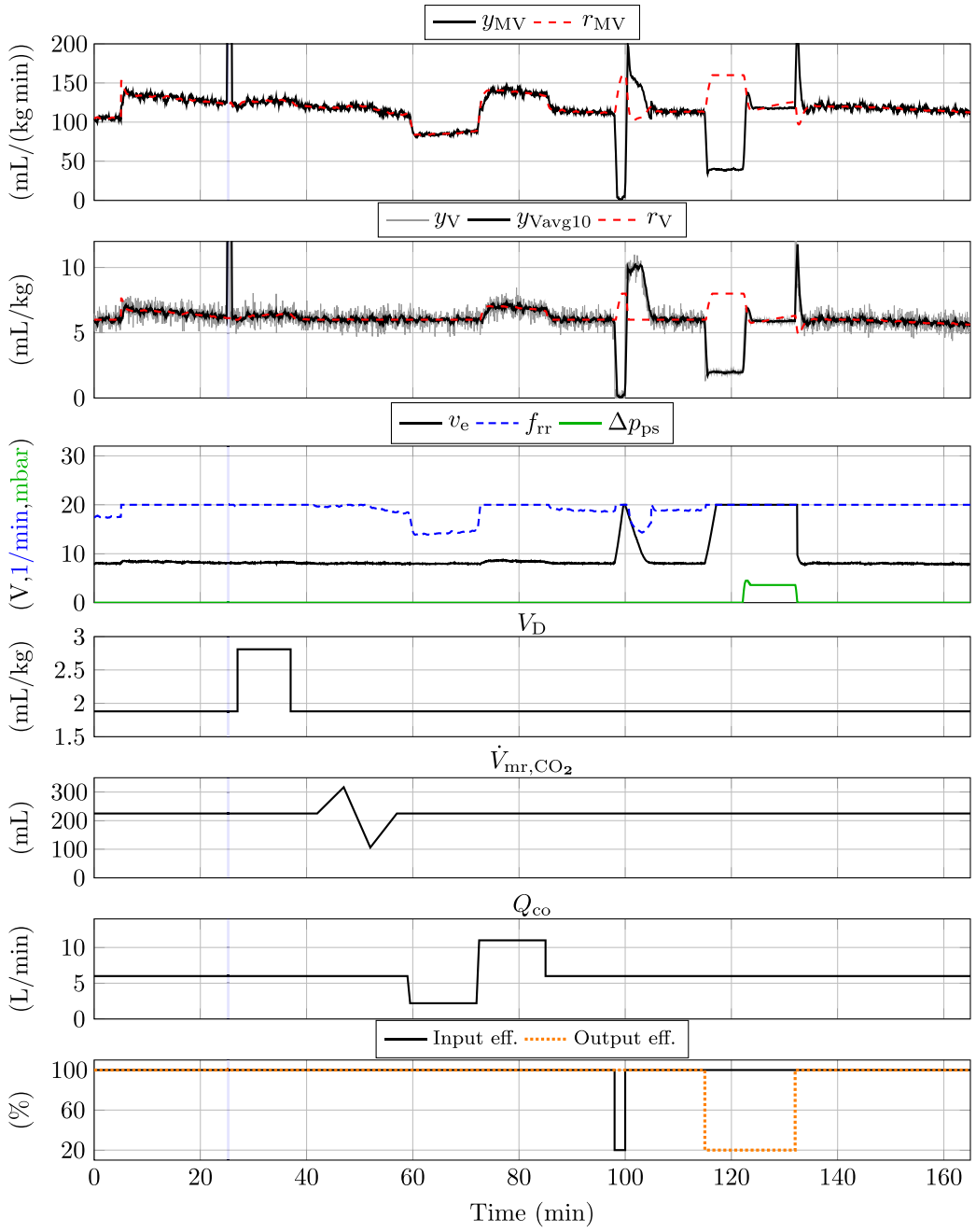

Fig. 11. Single simulated tidal volume response of the nominal parameter set. In the second graph, the gray curve denotes the unfiltered measurement. The blue area marks the disconnection event defined in Table A.1.

3. Results

3.1. Simulation

For the nominal virtual patient, the simulation results of the internal MV and V_t control loops are given in Fig. 11. y_{mv} followed r_{mv}, and while y_V is noisy, the 10-breath moving average filter y_{Vavg10} tracks r_V. The disconnection at $t = 25$ min does not affect y_V. During the reduction of PNS efficiency from $t = 98$ min to $t = 100$ min and from $t = 115$ min to $t = 132$ min, neither r_{mv} nor r_V were achieved, but in both cases, v_e increased to its limit of 20 V in 2 min.

When the reduced input PNS efficiency was restored at $t = 100$ min, the control system reduced f_{rr} while y_V remained at 9 mL/kg to 10 mL/kg, even though v_e continuously decreased. f_{rr} initially decreased but returned to 20 min^{-1} when r_V was tracked again at $t = 104$ min.

At $t = 122$ min, pressure support was activated, and both r_{mv} and r_V were tracked. When PNS efficiency increased back to 100% at $t = 132$ min, Δp_{ps} gradually decreased to zero, and v_e decreased to its steady-state value range in between 6.0 V and 6.5 V in 1 min.

Fig. 12 shows the CO_2 simulation results from all virtual patients of the scenario defined in Table A.1. The reference step of r_{CO_2} from 45 mmHg to 39 mmHg achieved a settling time ($P_{etCO_2} < 40$ mmHg) in all simulations in between 5.5 min and 14 min with a mean settling time of 9.0 min. Both changes in V_D and in $\dot{V}_{mr,CO_2}$ led to a change in y_{CO_2} of approximately 1 mmHg. During changes in Q_{co}, y_{CO_2} varied from r_{CO_2} up to 7 mmHg. After the input PNS efficiency was restored, y_{CO_2} tracked r_{CO_2} in less than 10 min. During decreased output PNS efficiency, y_{CO_2} increases up to the pressure support limit of 50 mmHg. Afterwards, y_{CO_2} decreased to 43 mmHg, and over 30 min, r_{CO_2} was reached. When the

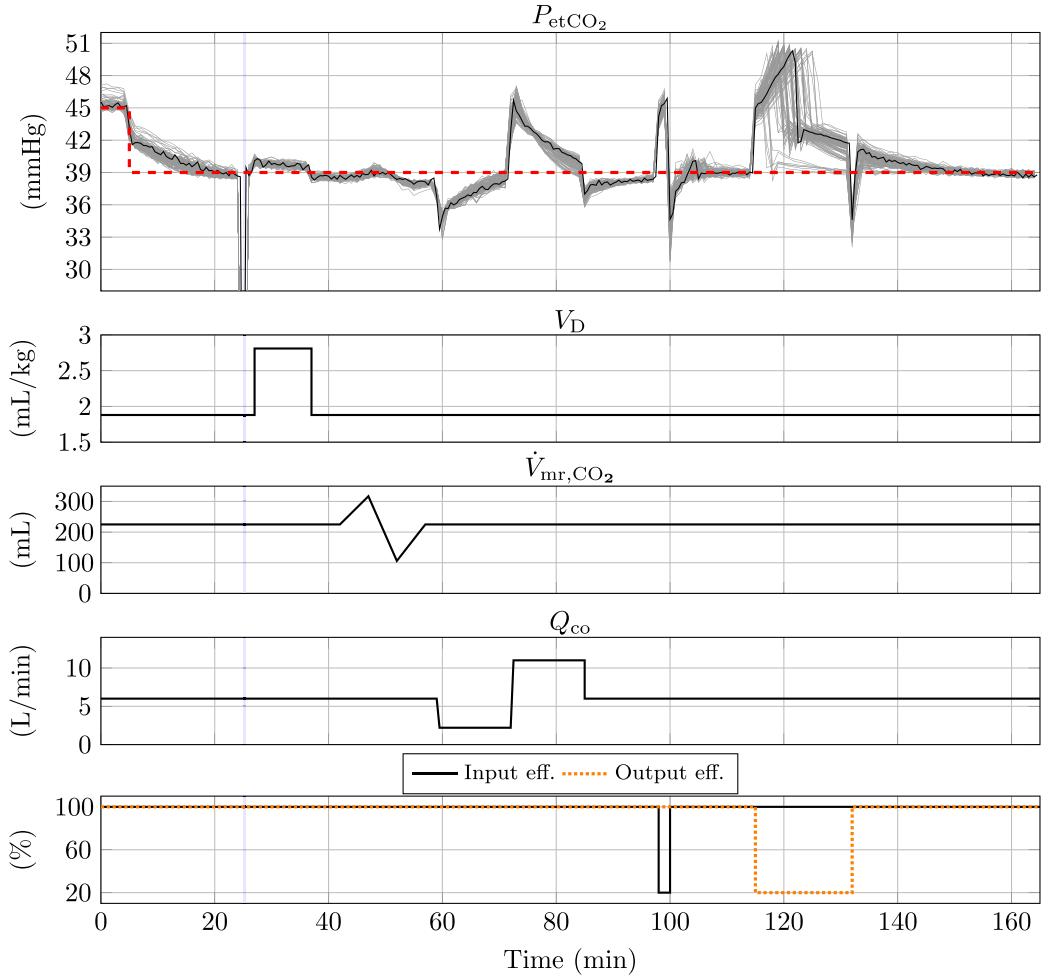

Fig. 12. Accumulated simulated y_{CO_2} of the nominal parameter set (black line) and 100 virtual patients (gray lines). The red dashed line denotes r_{CO_2}. The blue area marks the disconnection event defined in Table A.1.

Table 2
Stimulation patterns used in the animal trials. BIP denotes a biphasic pulse, in which the pulse voltage changes polarity within the pulse; ALT denotes an alternating pulse, in which the pulse polarity changes after each pulse.

Stim. pat.	T_{pw} (ms)	f_p (Hz)	T_s (s)	Pulse dir.
I	0.05	40	1	BIP
II	0.40	78	0.5	BIP
III	0.60	208	1	ALT
IV	1.00	143	1	BIP

output PNS efficiency increased back to 100%, y_{CO_2} decreased shortly but returned to its previous trend.

3.2. Animal trials

Two illustrative examples of reference tracking of MV and V_t during the animal trials are shown in Fig. 13. The control system was activated at $t = 0$ min. As shown in Fig. 13a, no pressure support was applied, and in the first 10 min, r_{MV} was tracked by increasing f_{rr}, while r_V was kept constant at 6 mL/kg. After saturation of f_{rr}, r_V increased according to the behavior defined in Eqs. (6), (7), and y_V followed by increasing v_e. In Fig. 13b, the pressure support controller was active while f_{rr} and v_e were saturated. The controller output variables did not overreact to the process noise in y_V.

Example responses of the MV and V_t control loops to disturbances are displayed in Fig. 14. In Fig. 14a, r_V was not achieved even when all actuators were saturated. At $t = 10$ min, the mechanical ventilator was disconnected from the animal's lungs. The applied pressure support did not decrease. At $t = 16$ min, the maximum f_{rr} was manually decreased from 30 min^{-1} to 28 min^{-1}, leading to an increased y_V so that r_V could be tracked and Δp_{ps} decreased. In Fig. 14b, the pig activated its respiratory muscles at approximately $t = 9$ min, leading to an increase in y_V, similar to an impulse disturbance.

Fig. 15 shows the offset of pressure support due to changing stimulation efficiency as the electrodes were relocated at approximately $t = 9$ min. Δp_{ps} decreased and r_V was followed, and at approximately $t = 15$ min, v_e started to decrease while f_{rr} was kept constant.

Fig. 16a shows a sample reference r_{CO_2} step without pressure support. At $t = 0$ s, r_{CO_2} was set to 39 mmHg. y_{CO_2} converged with r_{CO_2} after approximately 50 min. The corresponding minute volume, tidal volume, and controller outputs are shown in Fig. 13a. The y_{CO_2} response to the stimulation efficiency change in Fig. 15 is given in Fig. 16b. After stimulation efficiency increased, y_{CO_2} decreased from 44 mmHg to 38 mmHg in 2 min and gradually converged to the reference r_{CO_2}.

Table 3 shows the control performance for reference step changes during the animal trials. The settling time was defined as the duration at which y_{CO_2} differed less than 1 mmHg from r_{CO_2} and was between 8.25 min and 38.8 min. For PNS without pressure support, no overshoot was observed, while the maximum overshoot for PNS with pressure support was 1.3 mmHg.

Table 4 shows the closed-loop performance of disturbances during the animal trials. The compensation time was defined as the duration between the time at which the maximum error was recorded and the time at which y_{CO_2} reaches the 1 mmHg bound of r_{CO_2} for the first time.

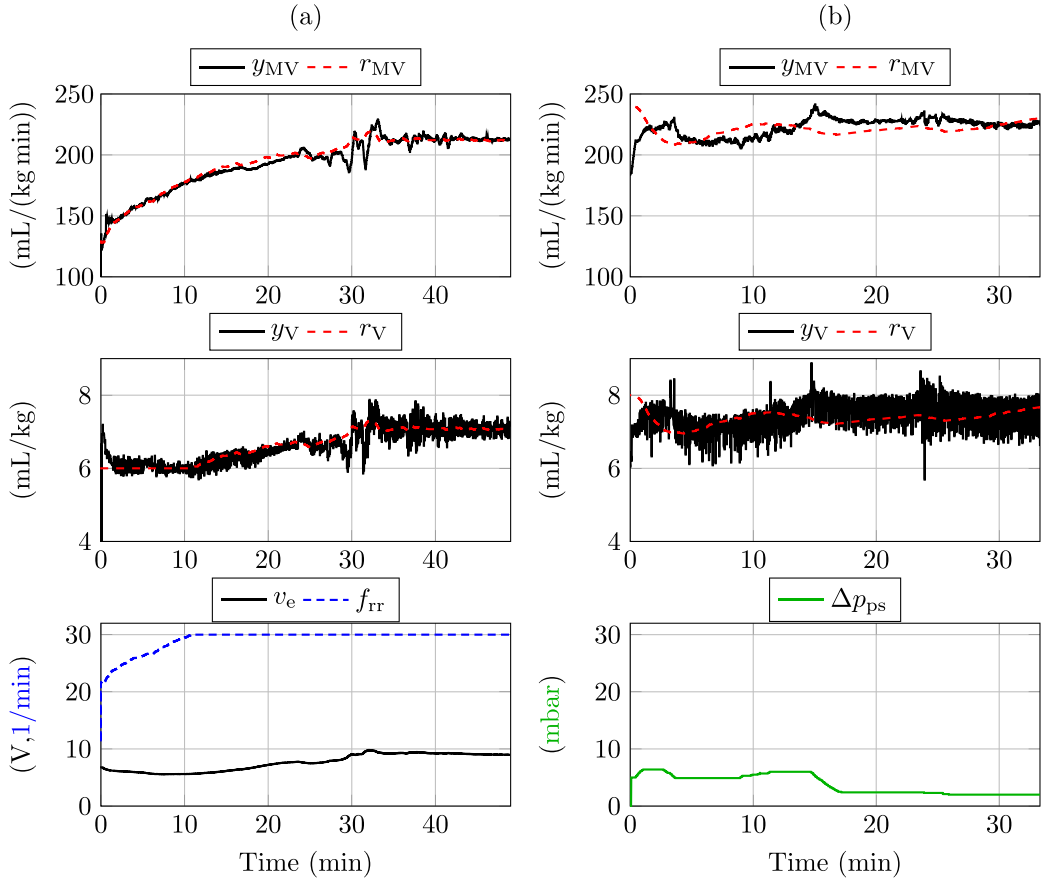

Fig. 13. Reference tracking of the MV and V_t loops without (a) and with (b) pressure support. For (b), f_{rr} was kept at $30\,\mathrm{min}^{-1}$ and v_e at its limit set to 14.0 V.

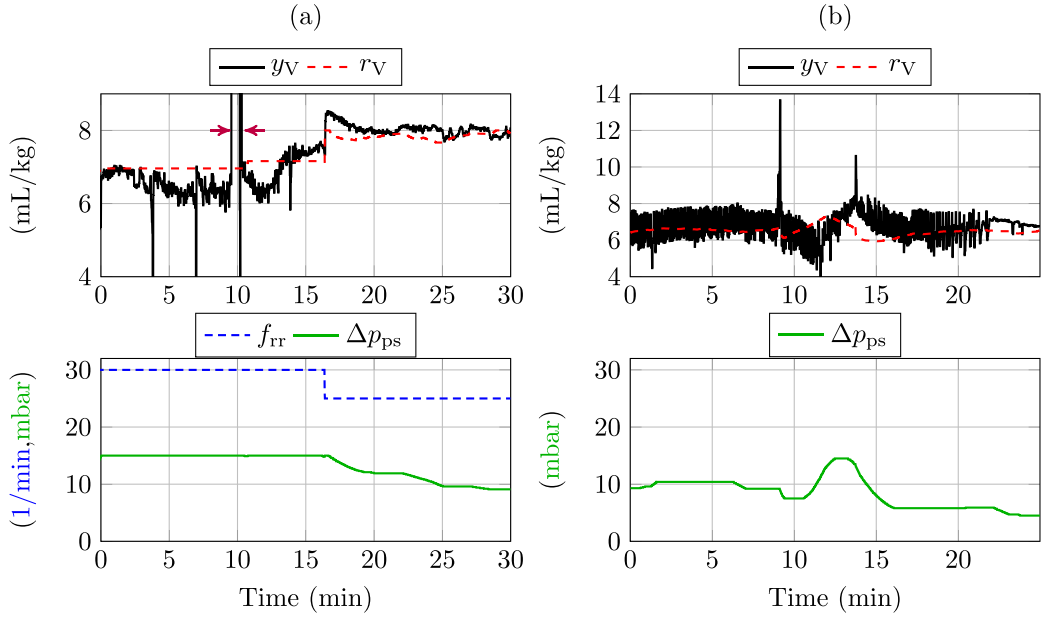

Fig. 14. Closed-loop disturbance response to (a) disconnection and secrete removal (arrows) and (b) the pig's own respiratory effort. It should be noted that the y-scales of the upper graphs are different. For (a), v_e was constant at 13.0 V, and for (b), f_{rr} was $30\,\mathrm{min}^{-1}$ and v_e was 13.0 V.

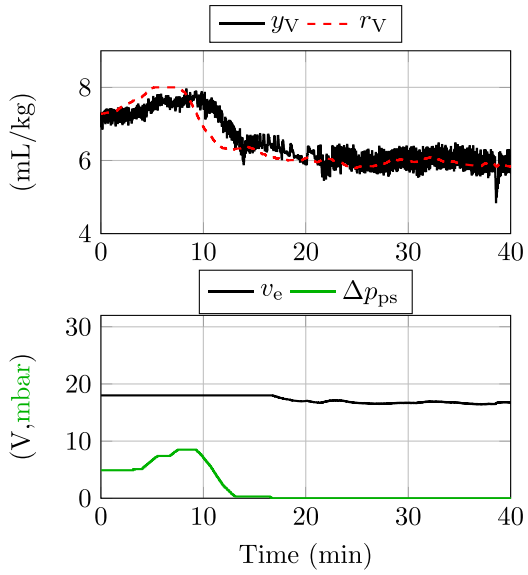

Fig. 15. Closed-loop response to a change in stimulation efficiency. f_{rr} was 30 min^{-1}.

Table 3
Performance of r_{CO_2} step responses during animal trials.

Pig	Initial y_{CO_2} (mmHg)	r_{CO_2} (mmHg)	Settling time (min)	Overshoot (mmHg)	Pressure support	Stim. pat.
1	46.2	39.0	38.8	0	Off	I
2	33.0	41.0	23.7	0.3	On	III
2	39.3	42.0	37.4	1.1	On	IV
3	43.0	39.0	32.0	0	Off	III
3	43.6	41.0	22.2	0	Off	III
4	41.5	45.0	8.25	0.7	On	II
4	44.3	41.0	30.7	1.3	On	II
5	40.7	45.0	7.3	0	Off	III

Table 4
Disturbance rejection performance of the animal trials.

Pig	Peak error (mmHg)	Compensation time (min)	Settling time (min)	Pressure support	Stim. pat.
1	11.6	25.9	31.7	On	III
2	3.67	2.33	2.33	On	IV
3	8.46	26.3	26.3	Off	III
3	6.59	5.72	5.72	On	III
3	3.53	1.80	20.3	On	III
3	2.53	2.05	22.0	On	III

Whereas disturbances with a magnitude below 7.00 mmHg had a compensation time of 5.72 min or less, disturbances above 8.00 mmHg had a compensation time of approximately 26 min. The maximum settling time was 31.7 min.

4. Discussion

A novel cascaded control system for PNS with optional pressure support to maintain CO_2 gas exchange was developed and validated. The control system demonstrated robustness in simulations of virtual patients with dynamically changed conditions and PNS effectiveness. To the best of our knowledge, this study shows the first reported closed-loop control of end-tidal partial pressure of CO_2 (P_{etCO_2}) in pigs and controlled in-vivo PNS for longer than 20 min. The control system was robust to real-world disturbances, including disconnections, the pig's own respiratory effort, and fluctuations in PNS effectiveness.

The P_{etCO_2} dynamics of the validation model and the recorded animal trials were different. For example, the time constant of P_{etCO_2} was faster in the validation model, which was designed with a gas exchange model for human subjects. In the animal trials, a pig was stimulated and mechanically ventilated. Therefore, different results are expected between the simulation and the animal trials. Even though the control response was slower in the animal trials, the ability to control both is further evidence of the control system's robustness.

Reported step responses in rats reached a steady state of P_{etCO_2} after approximately 15 min [14,17]. While our system reached steady state after similar durations in patient simulations, the settling time of our steps in pig trials from Table 3 reached almost 40 min. The time constants of CO_2 in rats may differ from those in pigs. Furthermore, the time constants depend on the physiological state of the animals. Another reason may be different prioritization during control design. The proposed system focused on disturbance rejection and robustness against dynamic changing conditions, leading to a lower performance in reference tracking.

The control system proposed by Siu et al. [14,17] incorporates a nonlinear fifth-order model comprising more than 20 parameters and a neural network with 72 neurons, resulting in a complex control system. In contrast, the proposed cascaded robust PI control structure was relatively simple and computationally less expensive, comprising only six control parameters. However, the control systems developed by Siu et al. and Zbrzeski et al. [16] generates a volume profile, while the present study focused exclusively on tidal volume control.

The PNS pattern shapes were defined in advance based on our previous studies [24]. This step can be automated if the automatic procedure proposed by Keogh et al. [10] is combined with the proposed control system.

Regarding limitations, the results of the animal trials were only exemplary. Since the primary objective of the animal trials was not controller validation, no systematic validation of the control system in animal trials was possible. However, the control system was statistically validated in simulations.

Because direct blood gas measurements were not available in real-time, we have used P_{etCO_2} as a surrogate parameter for the arterial partial CO_2 pressure, but they may differ depending on the individual patient [42]. If this control system is used on patients, the reference r_{CO_2} has to be set in such a way that the desired arterial partial CO_2 pressure is achieved.

The model developed to test controller robustness was not validated with the measurement data in its final form. However, the human gas exchange model is a slightly modified model from literature [33] with the dissociation curve from Spencer [34]. The GPR [31] and the physiological PNS model [32] were validated with pig measurement data. Therefore, the relationship between tidal volume and stimulation voltage may differ in humans.

This study demonstrated P_{etCO_2} control via PNS in pigs. Further, it was shown that pressure support can maintain gas exchange if PNS becomes unfeasible due to an unexpected event. The proposed control system can help develop systems applied in ICUs to prevent VIDD.

5. Conclusion

This study demonstrated a cascaded robust control system for P_{etCO_2}, minute volume, and tidal volume in PNS combined with mechanical ventilation via pressure support. The control system's robustness was validated in simulations and animal trials with pigs, which responded adequately to various disturbances and changes in the pig's conditions. Further developments may include the automation of PNS parameters and volume profiles. While the results are promising, further validation is required before the control system can be considered safe for use in humans. Nevertheless, the feasibility of the PNS control system demonstrated in this study may facilitate the development of PNS control systems suitable for the ICU.

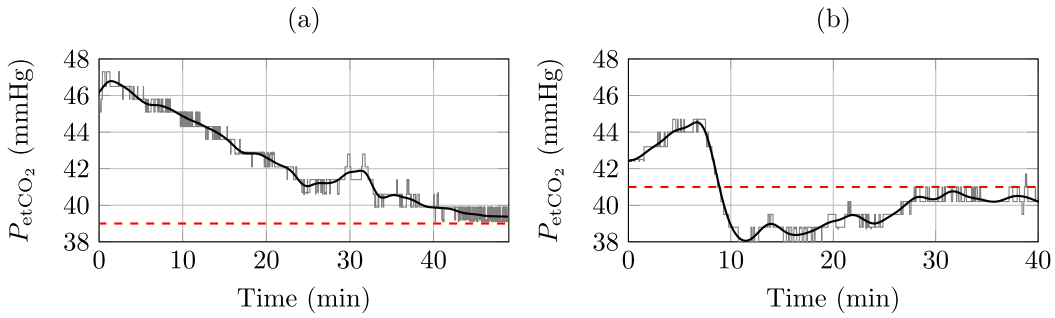

Fig. 16. Exemplary closed-loop response of y_{CO_2} to (a) an r_{CO_2} step and (b) stimulation efficiency change. The gray lines show the measurements, and the black line shows the low-pass filtered signal (3rd order with crossover frequency at 0.1 Hz). The dashed red line denotes the reference r_{CO_2}.

CRediT authorship contribution statement

Arnhold Lohse: Writing – review & editing, Writing – original draft, Visualization, Validation, Software, Methodology, Investigation, Formal analysis, Data curation, Conceptualization. **Felix Röhren:** Writing – review & editing, Investigation. **Philip von Platen:** Writing – review & editing, Methodology. **Carl-Friedrich Benner:** Writing – review & editing, Investigation. **Dmitrij Ziles:** Writing – review & editing, Resources, Investigation. **Marius Hühn:** Writing – review & editing, Resources, Investigation. **Matthias Manfred Deininger:** Writing – review & editing, Resources, Investigation. **Thomas Breuer:** Writing – review & editing, Supervision, Resources, Project administration, Investigation, Funding acquisition. **Steffen Leonhardt:** Writing – review & editing, Supervision, Project administration, Funding acquisition. **Marian Walter:** Writing – review & editing, Supervision, Project administration, Funding acquisition.

Ethics

The animal study was approved by the appropriate governmental institution (Landesamt für Natur, Umwelt und Verbraucherschutz Nordrhein-Westfalen, LANUV NRW, Germany, reference number: 81-02.04.2020.A080, approval date: 07.07.2020) and performed in accordance with German legislation governing animal studies following the "Guide for the care and use of Laboratory Animals" (NIH publication, 8th edition, 2011), the principles for care and use of animals based on the Helsinki declaration and the Directive 2010/63/EU on the protection of animals used for scientific purposes (Official Journal of the European Union, 2010). The experiments were carried out in the Institute for Laboratory Animal Science and Experimental Surgery of the RWTH University Hospital Aachen.

Declaration of generative AI and AI-assisted technologies in the writing process

During the preparation of this work the authors used Deepl Write (DeepL SE, Cologne, Germany) in order to improve language and readability. Afterwards, the authors reviewed and edited the content as needed and take full responsibility for the content of the published article.

Funding

The authors gratefully acknowledge funding by the Deutsche Forschungsgemeinschaft, Germany (DFG, German Research Foundation - 420664178, LE 817/39-1 and BR-5308/3-1).

Declaration of competing interest

The authors declare that they have no known competing financial interests or personal relationships that could have appeared to influence the work reported in this paper.

Table A.1
Scenario used to validate the control system.

Time (min)	Event description
5.0	Step of r_{CO_2} from 45 mmHg to 39 mmHg
25.0–25.5	Disconnection from the mechanical ventilator
27.0	Increase of V_D from 1.88 mL/kg to 2.81 mL/kg
37.0	Decrease of V_D to 1.88 mL/kg
42.0–47.0	Increase of $\dot{V}_{mr,CO_2}$ from 225 mL/min to 317 mL/min
47.0–52.0	Decrease of $\dot{V}_{mr,CO_2}$ to 106 mL/min
52.0–57.0	Increase of $\dot{V}_{mr,CO_2}$ to 225 mL/min
59.0–59.5	Decrease of Q_{co} from 6 L/min to 2.2 L/min
72.0–72.5	Increase of Q_{co} to 11 L/min
85.0	Decrease of Q_{co} back to nominal value of 6 L/min
98.0–100.0	Decrease of input PNS efficiency by 80%
115.0–132.0	Decrease of output PNS efficiency by 80%

Appendix A. Robustness validation scenario

See Table A.1.

Acronyms

GPR	Gaussian process regression
ICU	Intensive care unit
MV	Minute volume
PI	Proportional-integrative
PNS	Phrenic nerve stimulation
VIDD	Ventilator-induced diaphragmatic dysfunction

Appendix B. Supplementary data

Supplementary material related to this article can be found online at https://doi.org/10.1016/j.bspc.2025.107649.

Data availability

Data will be made available on request.

References

[1] J.-M. Boles, J. Bion, A. Connors, M. Herridge, B. Marsh, C. Melot, R. Pearl, H. Silverman, M. Stanchina, A. Vieillard-Baron, T. Welte, Weaning from mechanical ventilation, Eur. Respir. J. 29 (5) (2007) 1033–1056, http://dx.doi.org/10.1183/09031936.00010206.

[2] S.N.A. Hussain, M. Mofarrahi, I. Sigala, H.C. Kim, T. Vassilakopoulos, F. Maltais, I. Bellenis, R. Chaturvedi, S.B. Gottfried, P. Metrakos, G. Danialou, S. Matecki, S. Jaber, B.J. Petrof, P. Goldberg, Mechanical ventilation-induced diaphragm disuse in humans triggers autophagy, Am. J. Respir. Crit. Care Med. 182 (11) (2010) 1377–1386, http://dx.doi.org/10.1164/rccm.201002-0234OC.

[3] M. Dres, B.-P. Dubé, J. Mayaux, J. Delemazure, D. Reuter, L. Brochard, T. Similowski, A. Demoule, Coexistence and impact of limb muscle and diaphragm weakness at time of liberation from mechanical ventilation in medical intensive care unit patients, Am. J. Respir. Crit. Care Med. 195 (1) (2017) 57–66, http://dx.doi.org/10.1164/rccm.201602-0367OC.

[4] F.C. Trudzinski, B. Neetz, F. Bornitz, M. Müller, A. Weis, D. Kronsteiner, F.J. Herth, N. Sturm, V. Gassmann, T. Frerk, C. Neurohr, A. Ghiani, B. Joves, A. Schneider, J. Szecsenyi, S. Von Schumann, J. Meis, Risk factors for prolonged mechanical ventilation and weaning failure: A systematic review, Respir. 101 (10) (2022) 959–969, http://dx.doi.org/10.1159/000525604.

[5] A. Panelli, M.A. Verfuß, M. Dres, L. Brochard, S.J. Schaller, Phrenic nerve stimulation to prevent diaphragmatic dysfunction and ventilator-induced lung injury, Intensiv. Care Med. Exp. 11 (1) (2023) 94, http://dx.doi.org/10.1186/s40635-023-00577-5.

[6] A. Zbrzeski, R. Siu, Y. Bornat, B.K. Hillen, R. Jung, S. Renaud, A versatile fast-development platform applied to closed-loop diaphragmatic pacing, in: 2015 7th International IEEE/EMBS Conference on Neural Engineering, NER, IEEE, Montpellier, France, 2015, pp. 791–794, http://dx.doi.org/10.1109/NER.2015.7146742.

[7] L. Haviv, H. Friedman, U. Bierman, I. Glass, A. Plotkin, A. Weissbrod, S. Shushan, V. Bluvshtein, E. Aidinoff, N. Sobel, A. Catz, Using a sniff controller to self-trigger abdominal functional electrical stimulation for assisted coughing following cervical spinal cord lesions, IEEE Trans. Neural Syst. Rehabil. Eng. 25 (9) (2017) 1461–1471, http://dx.doi.org/10.1109/TNSRE.2016.2632754.

[8] I.G. Malone, M.N. Kelly, R.L. Nosacka, M.A. Nash, S. Yue, W. Xue, K.J. Otto, E.A. Dale, Closed-loop, cervical, epidural stimulation elicits respiratory neuroplasticity after spinal cord injury in freely behaving rats, Eneuro 9 (1) (2022) ENEURO.0426–21.2021, http://dx.doi.org/10.1523/ENEURO.0426-21.2021.

[9] Z. Zhou, W. Wang, R. Yang, Y. Wang, L. Zhu, Y. Huang, Bio-Z-based feedback-controlled external diaphragm pacing system, IEEE Trans. Circuits Syst. II 70 (8) (2023) 2779–2783, http://dx.doi.org/10.1109/TCSII.2023.3255902.

[10] C. Keogh, F. Saavedra, S. Dubo, P. Aqueveque, P. Ortega, B. Gomez, E. Germany, D. Pinto, R. Osorio, F. Pastene, A. Poulton, J. Jarvis, B. Andrews, J.J. FitzGerald, Closed-loop parameter optimization for patient-specific phrenic nerve stimulation, Artif. Organs. 48 (3) (2024) 274–284, http://dx.doi.org/10.1111/aor.14593.

[11] P. von Platen, A. Pomprapa, B. Lachmann, S. Leonhardt, The dawn of physiological closed-loop ventilation—a review, Crit. Care 24 (1) (2020) 121, http://dx.doi.org/10.1186/s13054-020-2810-1.

[12] Jin-Oh Hahn, G.A. Dumont, J.M. Ansermino, System identification and closed-loop control of end-tidal CO2 in mechanically ventilated patients, IEEE Trans. Inf. Technol. Biomed. 16 (6) (2012) 1176–1184, http://dx.doi.org/10.1109/TITB.2012.2204067.

[13] W. Ai, V. Suresh, P.S. Roop, Development of closed-loop modelling framework for adaptive respiratory pacemakers, Comput. Biol. Med. 141 (2022) 105136, http://dx.doi.org/10.1016/j.compbiomed.2021.105136.

[14] R. Siu, J.J. Abbas, B.K. Hillen, J. Gomes, S. Coxe, J. Castelli, S. Renaud, R. Jung, Restoring ventilatory control using an adaptive bioelectronic system, J. Neurotrauma 36 (24) (2019) 3363–3377, http://dx.doi.org/10.1089/neu.2018.6358.

[15] R.Z. Adury, R. Siu, R. Jung, Co-activation of the diaphragm and external intercostal muscles through an adaptive closed-loop respiratory pacing controller, Front. Rehabil. Sci. 4 (2023) 1199722, http://dx.doi.org/10.3389/fresc.2023.1199722.

[16] A. Zbrzeski, Y. Bornat, B. Hillen, R. Siu, J. Abbas, R. Jung, S. Renaud, Bio-inspired controller on an FPGA Applied to closed-loop diaphragmatic stimulation, Front. Neurosci. 10 (2016) http://dx.doi.org/10.3389/fnins.2016.00275.

[17] R. Siu, J.J. Abbas, D.D. Fuller, J. Gomes, S. Renaud, R. Jung, Autonomous control of ventilation through closed-loop adaptive respiratory pacing, Sci. Rep. 10 (1) (2020) 21903, http://dx.doi.org/10.1038/s41598-020-78834-w.

[18] E.P. Judge, J.M.L. Hughes, J.J. Egan, M. Maguire, E.L. Molloy, S. O'Dea, Anatomy and bronchoscopy of the porcine lung. a model for translational respiratory medicine, Am. J. Respir. Cell. Mol. Biol. 51 (3) (2014) 334–343, http://dx.doi.org/10.1165/rcmb.2013-0453TR.

[19] P.M. Reardon, J. Wong, A. Fitzpatrick, E.C. Goligher, Diaphragm function in acute respiratory failure and the potential role of phrenic nerve stimulation, Curr. Opin. Crit. Care 27 (3) (2021) 282–289, http://dx.doi.org/10.1097/MCC.0000000000000828.

[20] X.J. Frawley, S.A. Yong, Ventilatory support in the intensive care unit, Anaesth. Intensiv. Care Med. 23 (10) (2022) 620–627, http://dx.doi.org/10.1016/j.mpaic.2022.08.001.

[21] M.M. Deininger, D. Ziles, A. Borleis, T. Seemann, F. Erlenkoetter, C. Bleilevens, A. Lohse, C.-F. Benner, S. Leonhardt, M. Walter, T. Breuer, Breath-by-breath comparison of a novel percutaneous phrenic nerve stimulation approach with mechanical ventilation in juvenile pigs: A pilot study, Sci. Rep. 14 (1) (2024) 10252, http://dx.doi.org/10.1038/s41598-024-61103-5.

[22] A. Serpa Neto, S.O. Cardoso, J.A. Manetta, V.G.M. Pereira, D.C. Espósito, M.D.O.P. Pasqualucci, M.C.T. Damasceno, M.J. Schultz, Association between use of lung-protective ventilation with lower tidal volumes and clinical outcomes among patients without acute respiratory distress syndrome: A meta-analysis, JAMA 308 (16) (2012) 1651, http://dx.doi.org/10.1001/jama.2012.13730.

[23] B. Parvinian, C. Scully, H. Wiyor, A. Kumar, S. Weininger, Regulatory considerations for physiological closed-loop controlled medical devices used for automated critical care: Food and drug administration workshop discussion topics, Anesth. Analg. 126 (6) (2018) 1916–1925, http://dx.doi.org/10.1213/ANE.0000000000002329.

[24] A. Lohse, P. Von Platen, C.-F. Benner, M.M. Deininger, T.G. Seemann, D. Ziles, T. Breuer, S. Leonhardt, M. Walter, Evaluation of electric phrenic nerve stimulation patterns for mechanical ventilation: A pilot study, Sci. Rep. 13 (1) (2023) 11303, http://dx.doi.org/10.1038/s41598-023-38316-1.

[25] K.J. Åström, T. Hägglund, K.J. Åström, PID Controllers, second ed., International Society for Measurement and Control, Research Triangle Park, N.C, 1995.

[26] D.E. Seborg, Process Dynamics and Control, fourth ed., Wiley, Hoboken, NJ, 2017.

[27] J.B. West, A. Luks, West's Respiratory Physiology: The Essentials, tenth ed., Wolters Kluwer, Philadelphia, 2016.

[28] W. Fincham, F. Tehrani, A mathematical model of the human respiratory system, J. Biomed. Eng. 5 (2) (1983) 125–133, http://dx.doi.org/10.1016/0141-5425(83)90030-4.

[29] A. Saltelli (Ed.), Global Sensitivity Analysis: The Primer, Wiley, Chichester, West Sussex, 2008.

[30] S. Skogestad, I. Postlethwaite, Multivariable Feedback Control: Analysis and Design, second ed., John Wiley, Hoboken, NJ, 2005.

[31] A. Lohse, P. Von Platen, C.-F. Benner, S. Leonhardt, M.M. Deininger, D. Ziles, T. Seemann, T. Breuer, M. Walter, Identification of the tidal volume response to pulse amplitudes of phrenic nerve stimulation using Gaussian process regression, in: 2022 44th Annual International Conference of the IEEE Engineering in Medicine & Biology Society, EMBC, IEEE, Glasgow, Scotland, United Kingdom, 2022, pp. 135–138, http://dx.doi.org/10.1109/EMBC48229.2022.9871563.

[32] A. Lohse, M.M. Deininger, J. Loeser, F. Roehren, D. Ziles, T. Breuer, S. Leonhardt, M. Walter, A physiological model of phrenic nerve excitation by electrical stimulation, Biomed. Phys. Eng. Express 10 (2) (2024) 025017, http://dx.doi.org/10.1088/2057-1976/ad1fa3.

[33] J.J. Batzel, Cardiovascular and respiratory systems: Modeling, analysis, and control, Frontiers in Applied Mathematics, SIAM, Soc. for Industrial and Applied Mathematics, Philadelphia, Pa, 2007, no. 34.

[34] J.L. Spencer, E. Firouztale, R.B. Mellins, Computational expressions for blood oxygen and carbon dioxide concentrations, Ann. Biomed. Eng. 7 (1) (1979) 59–66, http://dx.doi.org/10.1007/BF02364439.

[35] A. Lohse, P. Von Platen, Steffen Leonhardt, M. Walter, Robust control of oxygen saturation during mechanical ventilation, Lékař a Tech. - Clin. Technol. (2024) 5–11, http://dx.doi.org/10.14311/CTJ.2024.1.01.

[36] F.S. Grodins, J. Buell, A.J. Bart, Mathematical analysis and digital simulation of the respiratory control system, J. Appl. Physiol. 22 (2) (1967) 260–276, http://dx.doi.org/10.1152/jappl.1967.22.2.260.

[37] K.D. Pagana, T.J. Pagana, Mosby's Manual of Diagnostic and Laboratory Tests, fifth ed., Elsevier Mosby, St. Louis, Missouri, 2014.

[38] P.H. Quanjer, G.J. Tammeling, J.E. Cotes, O.F. Pedersen, R. Peslin, J.-C. Yernault, Lung volumes and forced ventilatory flows, Eur. Respir. J. 6 (Suppl 16) (1993) 5–40, http://dx.doi.org/10.1183/09041950.005s1693.

[39] S.N. Stapel, H.-J.S. De Grooth, H. Alimohamad, P.W.G. Elbers, A.R.J. Girbes, P.J.M. Weijs, H.M. Oudemans-van Straaten, Ventilator-derived carbon dioxide production to assess energy expenditure in critically ill patients: Proof of concept, Crit. Care 19 (1) (2015) 370, http://dx.doi.org/10.1186/s13054-015-1087-2.

[40] M. Sundström, I. Tjäder, O. Rooyackers, J. Wernerman, Indirect calorimetry in mechanically ventilated patients. A systematic comparison of three instruments, Clin. Nutr. 32 (1) (2013) 118–121, http://dx.doi.org/10.1016/j.clnu.2012.06.004.

[41] J. Gonzalez, C. Delafosse, M. Fartoukh, A. Capderou, C. Straus, M. Zelter, J.-P. Derenne, T. Similowski, Comparison of bedside measurement of cardiac output with the thermodilution method and the Fick method in mechanically ventilated patients, Crit. Care 7 (2) (2003) 171, http://dx.doi.org/10.1186/cc1848.

[42] K. Satoh, A. Ohashi, M. Kumagai, M. Sato, A. Kuji, S. Joh, Evaluation of differences between $PaCO_2$ and $ETCO_2$ by age as measured during general anesthesia with patients in a supine position, J. Anesthesiol. 2015 (2015) 1–5, http://dx.doi.org/10.1155/2015/710537.